Telomerase reverse transcriptase is required for resistance to mycobacterial infection

Darryl JY Han [1], David M Costa [1], Geyang Luo [2], Kathryn Wright [3], Manitosh Pandey [1], Denise Wee [1], Yao Chen [1], Semih Can Akincilar [4], Vinay Tergaonkar [4], Rajkumar Dorajoo [5,6], Guillaume Carissimo [1,6], Amit Singhal [1,7], Philip M Elks [8], Pamela S Ellis [9], Catarina M Henriques [9], Bo Yan [2], Serge Mostowy [3], Stefan H Oehlers [1,7]*

[1] A*STAR Infectious Diseases Labs (A*STAR ID Labs), Agency for Science, Technology and Research (A*STAR), Singapore, Singapore.
[2] Center for Tuberculosis Research, Shanghai Public Health Clinical Center, Fudan University, Shanghai, People's Republic of China.
[3] Department of Infection Biology, London School of Hygiene & Tropical Medicine, London, United Kingdom.
[4] Laboratory of NF-κB Signalling, Institute of Molecular and Cell Biology (IMCB), Agency for Science, Technology and Research (A*STAR), Singapore, Singapore.
[5] Genome Institute of Singapore (GIS), Agency for Science, Technology and Research (A*STAR), Singapore.
[6] Yong Loo Lin School of Medicine, National University of Singapore, Singapore.
[7] Lee Kong Chian School of Medicine, Nanyang Technological University, Singapore.
[8] The Bateson Centre, School of Medicine and Population Health, Faculty of Health, University of Sheffield, Sheffield, United Kingdom.
[9] The Bateson Centre, MRC-Arthritis Research UK Centre for Integrated Research Into Musculoskeletal Ageing (CIMA) and Healthy Lifespan Institute (HELSI), School of Medicine and Population Health, University of Sheffield, Sheffield, UK.
* Corresponding author contact: stefan_oehlers@a-star.edu.sg

Character count: 47801

Abstract

Age is an important risk factor for infections such as tuberculosis (TB). Telomerase is expressed in immune cells yet leukocyte telomere length declines during ageing suggesting an age-dependent loss of telomerase activity in the immune system. Leukocyte telomere length has been correlated with worse outcomes in TB patients, however the mechanisms linking telomere biology to TB susceptibility and response to therapy are unexplored. Here we use the zebrafish-*Mycobacterium marinum* model to investigate the role of telomerase in TB resistance. We find depletion and inhibition of Tert, the catalytic subunit of telomerase, increases bacterial burden in zebrafish embryos. The Tert depletion infection susceptibility phenotype could not be rescued by p53 or STING depletion suggesting a non-canonical role for Tert in controlling mycobacterial infection. Consistent with a previously described role for Tert in developmental hematopoiesis, we find Tert is necessary for demand-driven emergency myelopoiesis to support containment of extended mycobacterial infection. Our findings establish a previously undescribed role for host telomerase in supporting infection demand-driven hematopoiesis to control infection.

Introduction

Ageing is one of the most important risk factors for tuberculosis (TB) susceptibility and severity (*1*). Animal models and clinical measurements have identified inflammageing, a persistent low grade interferonopathy triggered by accumulated DNA damage, and immune anergy, caused qualitatively by declining lymphocyte function and quantitatively by the biased production of myeloid cells, as potential mechanisms underlying age-dependent TB susceptibility (*2, 3*). Recent work across guinea pig and human systems

have demonstrated that TB accelerates ageing suggesting that *Mycobacterium tuberculosis* may actively benefit from accelerated host ageing and that interception of this process could yield novel targeted adjunctive therapies for an important at-risk group (*4*).

Leukocyte telomere length (LTL) decreases during ageing and influences immune function, specifically affecting susceptibility to infectious diseases driven by host immunopathology including TB (*5-12*). Some aspects of the relationship between LTL and TB biology may be ethnicity specific as while South African patients with longer LTL are more likely to have a successful response to TB treatment, South East Asian and East Asian patients with longer LTL experienced more treatment side effects (*13-15*). As telomerase activity is required for maintenance of LTL, we hypothesized decreased leukocyte expression of the telomerase reverse transcriptase (Tert) may drive the increased susceptibility of the elderly and those with short LTL to mycobacterial infection.

Expression of *tert* by hematopoietic stem cells is necessary for telomere elongation and likely protects chromosomes during hematopoiesis. There is an increasing body of evidence that Tert and the RNA template *TERC* execute important non-canonical functions in immunity as an inflammation-responsive gene aiding the expression of key hematopoietic differentiation genes (*16-18*). Telomerase-expressing macrophages (T-MACS) have been previously described and loss of telomerase expression has been associated with reduced immune cell-autonomous function (*19, 20*).

Here we utilize the zebrafish-*M. marinum* model of human TB to study the role of Tert in mycobacterial infection. We find that Tert is expressed at the site of infection and loss of Tert is causes reduced control of infection. Tert mRNA supplementation restores infection-induced, demand-driven hematopoiesis, highlighting the role of Tert in supporting hematopoietic resilience during chronic infection.

Results

Telomerase reverse transcriptase is expressed at the host-mycobacterial interface

To determine if T-MACs are present in mycobacterial granulomas we analyzed a previously published scRNAseq dataset of dissected zebrafish-*M. marinum* granulomas (*21*). We found *tert* is most expressed in proliferative cells, as expected from canonical function in telomere elongation of proliferating cells and matching the expression of the DNA polymerase subunit *pola2* (Figure 1A). Expression of *tert* was detected in myeloid-derived macrophage subsets, many of which lacked *pola2* expression suggesting a non-proliferative role of *tert* expression. There appeared to be comparable levels of *tert* expression across epithelialized macrophages (Epmacs, Cluster 3, and cdh1+ve) which make up the ring-like structure of mature granulomas compared to the “non-structural” myeloid cells (monocytes, inflammatory macrophages, DCs). The overall level of *tert* expression in the myeloid cell clusters was less than half of the level of *tert* expression proliferating cell clusters.

We analyzed the expression of *tert* in adult zebrafish-*M. marinum* granulomas by *in situ* hybridization and found expression in both the flat inner layer of primarily macrophage-derived epithelialized cells and in round cells around the periphery of the granuloma, presumably the proliferating cells identified in the scRNAseq dataset or monocyte-derived cells (Figure 1B). As expected from the heterogenous nature of previously described T-MACs, there were fewer *tert* positive cells detected within granulomas than were seen in previously published images of macrophages visualized with the pan monocyte marker *mpeg1* illustrating expression only in a subset of macrophages (*22*).

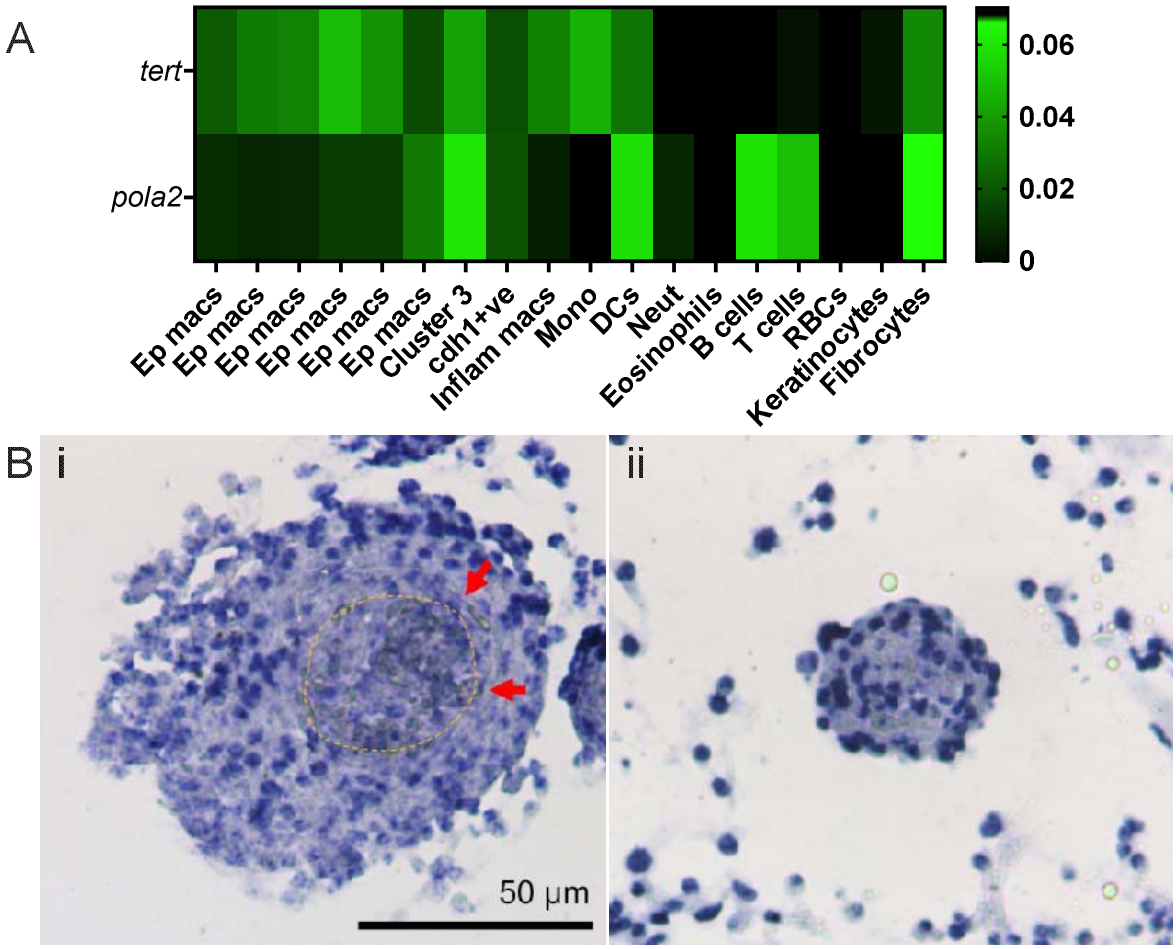

Figure 1: A subset of zebrafish macrophages express *tert* in mycobacterial granulomas. (A) Mean expression value of *tert* and *pola2* across clusters of granuloma cells identified by scRNAseq of adult zebrafish-*M. marinum* granulomas from (*21*).
(B) Detection of *tert* expression (blue staining) in (i) necrotic and (ii) cellular non-necrotic adult zebrafish-*M. marinum* granulomas by *in situ* hybridization. Yellow dashed line indicates edge of necrotic core and red arrows indicate epithelioid macrophage layer.

Telomerase deficiency increases the severity of pathogenic mycobacterial infection

We investigated the transcriptional regulation of *tert* following infection by whole embryo RT-qPCR and did not observe changes to *tert* transcription following *M. marinum* infection in developing zebrafish embryos (Supplementary Figure 1A).

We next examined the role of *tert* in the immune response to mycobacterial infection by knocking down expression with a pooled gRNA-CRISPR approach (Supplementary Figure 1B). Knockdown of *tert* increased *M. marinum* burden in zebrafish larvae at 5 days post infection (dpi) (Figure 2A). Our pooled gRNA-CRISPR approach reduced the telomeric repeat amplification protocol (TRAP) activity of whole embryo lysate demonstrating reduced canonical Tert function (Figure 2B). Consistent with telomere shortening being an age-dependent phenotype manifesting over months in zebrafish models, we did not observe any change to telomere length by whole body aggregate qPCR (Supplementary Figure 1C)

In contrast, infection with two relatively non-pathogenic mycobacteria, *Mycobacterium smegmatis* and smooth colony variant *Mycobacterium abscessus*, was comparable between scramble control and *tert* crispant embryos (Figure 2C and 2D). Infection with the more virulent rough colony variant *M. abscessus* resulted in higher bacterial burden in *tert* crispant embryos (Figure 2E). These data suggest the mycobacterial infection susceptibility is specific to infections capable of forming persistent inflammatory lesions.

We next tested the ability of *tert* crispants to control Chikungunya virus (CHIKV) infection, a well characterized wide host range RNA virus capable of replicating in zebrafish embryos (*23*). Quantification of infected cell area by fluorometry revealed comparable CHIKV infection levels between scramble control and *tert* crispant embryos, demonstrating a specific immune defect to infection by pathogenic bacteria (Figure 2F).

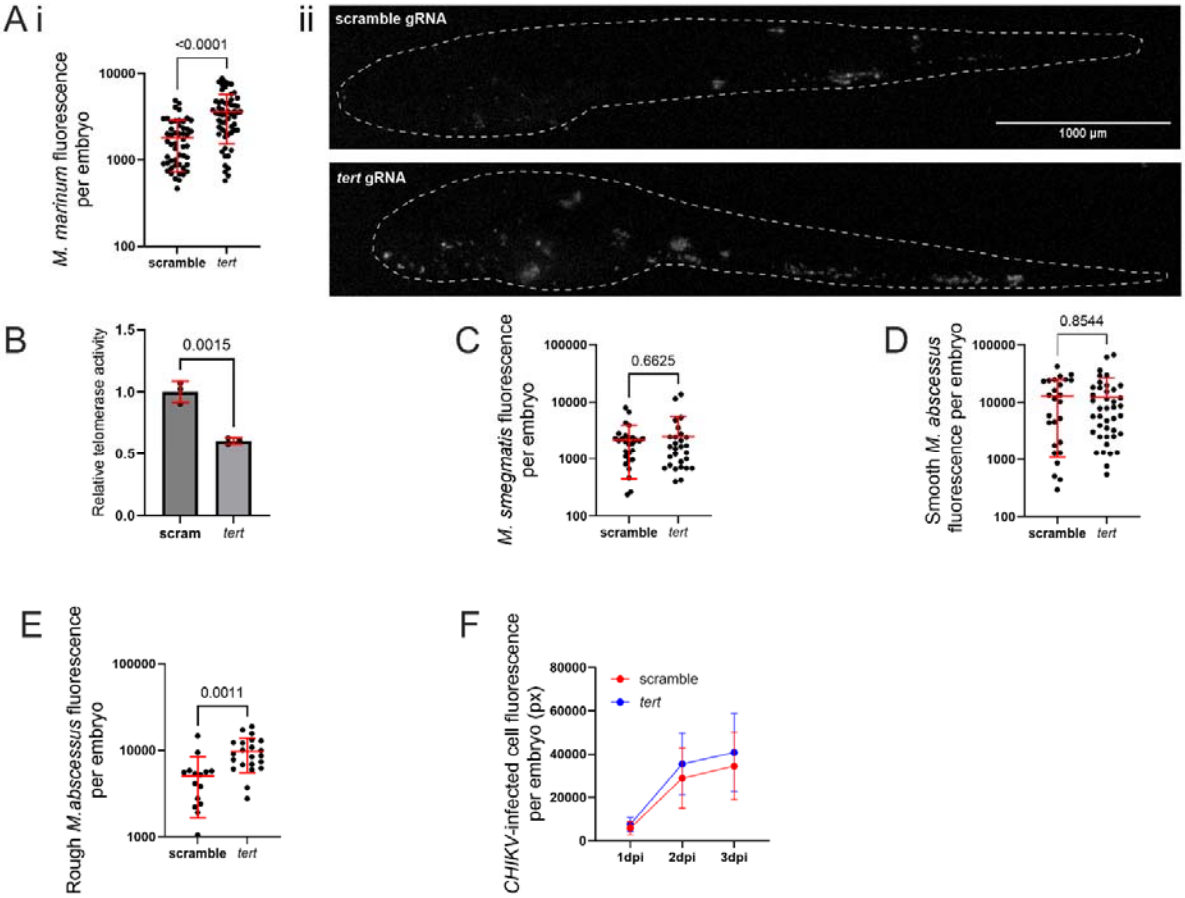

Figure 2: Knockdown of *tert* increases zebrafish susceptibility to pathogenic mycobacterial infection

(A) i. Quantification of *M. marinum* burden in 5 dpi *tert* crispant embryos. ii. Representative images of fluorescent *M. marinum* signal in 5 dpi *tert* crispant embryos. Dashed lines indicate outline of embryos.

(B) TRAP quantification of relative telomerase activity in 5 dpi *tert* crispant embryos.

(C) Quantification of *M. smegmatis* burden in 3 dpi *tert* crispant embryos.

(D) Quantification of smooth *M. abscessus* burden in 6 dpi *tert* crispant embryos.

(E) Quantification of rough *M. abscessus* burden in 6 dpi *tert* crispant embryos

(F) Quantification of CHIKV infected cells in 1-3 dpi *tert* crispant embryos (n= 29 scramble, n= 35 *tert* crispants).

Loss of the *telomerase RNA component* (*terc*) does not affect mycobacterial infection susceptibility

We complemented our analysis of *tert* by investigating *terc* dynamics and function during *M. marinum* infection in control and *tert*-deficient crispant embryos. We observed a decrease in *terc* levels during mycobacterial infection independent of *tert* status (Supplementary Figure 2A). Knockdown of *terc* using morpholino antisense oligonucleotides reduced the level of *terc* to 24.3 ± 7.1% (n = 4) of control levels (Supplementary Figure 2B) (*17*). However, we did not observe any effect of *terc* knockdown on *M. marinum* infection burden at 5 dpi (Supplementary Figure 2C). Previous reports had demonstrated a role for *terc* in supporting myelopoiesis (*17*), however we did not observe any effect of *terc* knockdown on neutrophil numbers in our infection system (Supplementary Figure 2D). We hypothesized that this was an effect of morpholino dilution allowing a small but sufficient amount of *terc* to escape blockade as the morpholinos were able to reduce early steady state myelopoiesis at 3 days post fertilization (Supplementary Figure 2E), but not late stead state myelopoiesis at 7 days post fertilization equivalent to our 5 dpi timepoint (Supplementary Figure 2F), or total neutrophil numbers (Supplementary Figure 2G).

Inhibition of telomerase reverse transcriptase increases infection susceptibility and overexpression is protective

We complemented our CRISPR-Cas9 knockdown approach with small molecule TERT inhibitors BIBR1532 and MST-312 (*24, 25*). Treatment of infected embryos increased *M. marinum* burden consistent with our genetic approach data (Figure 3A and 3B).

Overexpression of *tert* by microinjection with mRNA encoding zebrafish *tert* also reduced *M. marinum* burden (Figure 3C). Interestingly, supplementation of catalytically dead “VAA” *tert* mRNA reduced *M. marinum* burden (Supplementary File 1) (*20*). Analysis of Tert activity by TRAP found increased Tert activity in embryos injected with zebrafish *tert* mRNA but not with “VAA” *tert* mRNA (Figure 3D), suggesting a non-canonical function of Tert could be protective against infection by pathogenic mycobacteria. We further explored the effect of 3′ fragments of *tert* mRNA containing only the C terminus domain (CTD) of the predicted protein (Supplementary File 1), and found a protective effect of overexpression consistent with a non-canonical Tert function (Figure 3E).

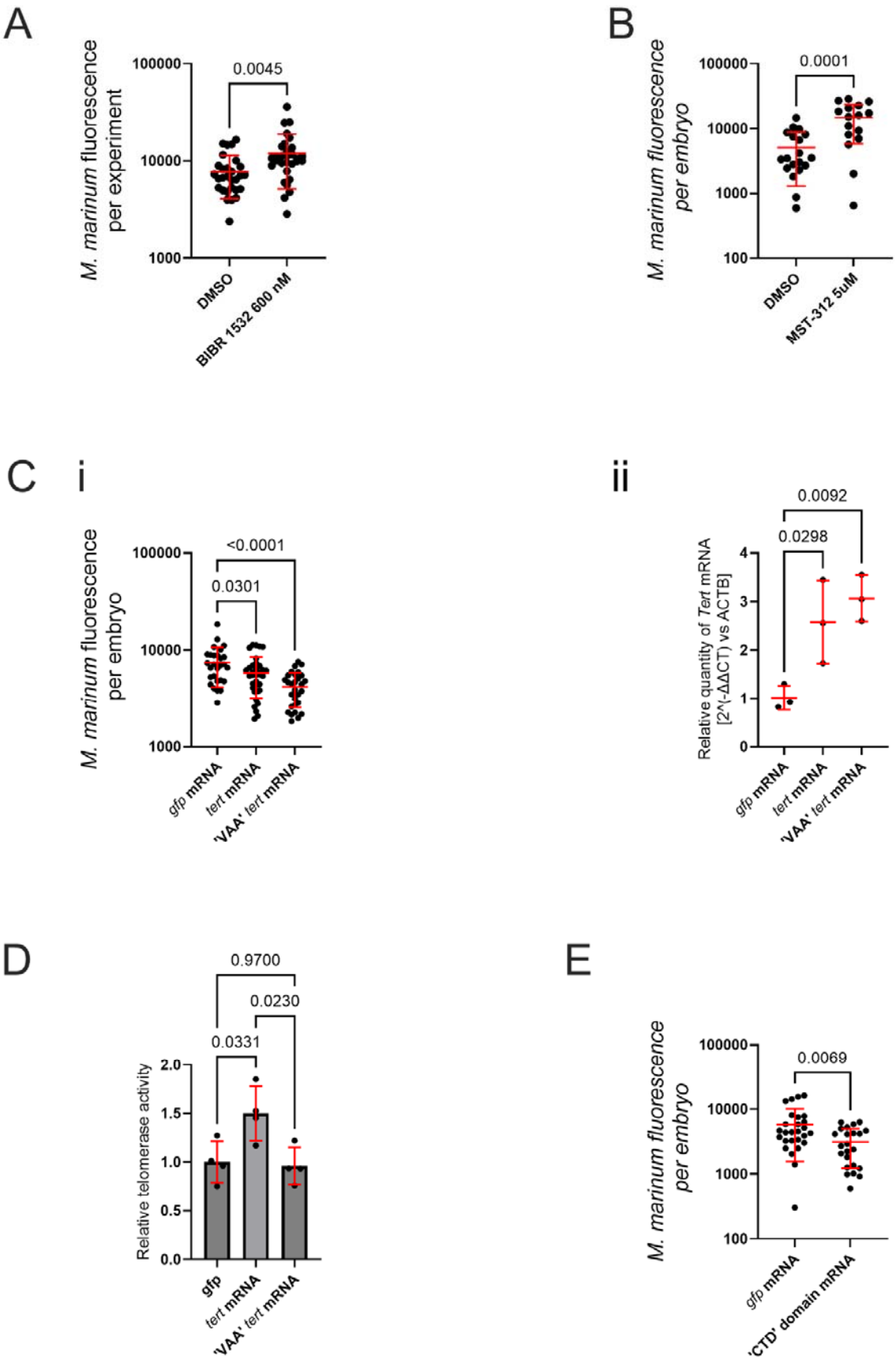
A
M. marinum fluorescence per experiment
100000
10000
1000
0.0045
DMSO
BIBR 1532 600 nM
B
M. marinum fluorescence per embryo
100000
10000
1000
100
0.0001
DMSO
MST-312 5uM
C
i
M. marinum fluorescence per embryo
100000
10000
1000
<0.0001
0.0301
gfp mRNA
tert mRNA
'VAA' tert mRNA
ii
Relative quantity of Tert mRNA [2^(-ΔΔCT) vs ACTB]
0.0092
0.0298
4
3
2
1
0
gfp mRNA
tert mRNA
'VAA' tert mRNA
D
Relative telomerase activity
0.9700
0.0230
0.0331
2.0
1.5
1.0
0.5
0.0
gfp
tert mRNA
'VAA' tert mRNA
E
M. marinum fluorescence per embryo
100000
10000
1000
100
0.0069
gfp mRNA
'CTD' domain mRNA

Figure 3: Small molecule and genetic inhibition of Tert increases susceptibility to mycobacterial infection while activation increases resistance to mycobacterial infection.
(A) Quantification of *M. marinum* burden in 5 dpi embryos treated with BIBR1532.
(B) Quantification of *M. marinum* burden in 5 dpi embryos treated with MST-312.
(C) i. Quantification of *M. marinum* burden in 5 dpi embryos injected with control *gfp*, *tert*, or VAA *tert* mRNA. ii. Quantification of *tert* transcript abundance in 1 dpf embryos injected with control *gfp*, *tert*, or VAA *tert* mRNA.
(D) TRAP quantification of relative telomerase activity in 5 dpi *tert* and VAA *tert* mRNA-injected embryos.
(E) Quantification of *M. marinum* burden in 5 dpi embryos injected with control *gfp* or C-terminal domain (CTD) *tert* mRNA.

Canonical DNA damage responses do not drive susceptibility to infection in *tert* crispants

Chronic infections reduce LTL and DNA damage-induced interferonopathy plays a critical role in TB pathogenesis (*26, 27*), however previous reports have demonstrated Tert-dependent telomere shortening is only observed in adult zebrafish and not at the embryo stage (*16, 28, 29*). We next investigated the hypothesis that canonical telomere-protective functions of Tert were necessary for resistance to *M. marinum* infection in the context of an increased genotoxic microenvironment caused by infection. Consistent with the presence of an increase in senescent cells, we observed SPiDER-βGal staining around *M. marinum* granulomas demonstrating the presence of the senescent cell marker beta galactosidase activity (Figure 4A).

Damage to chromosomal DNA has been demonstrated to activated Tp53-mediated growth restriction and Sting-mediated inflammation to accelerate aging phenotypes in Tert deficient adult zebrafish (*30, 31*). We hypothesized arrest of host immune cell proliferation and Sting-mediated production of type I interferons would be detrimental to control of *M. marinum* infection. Expression of the DNA damage response gene *tp53* was increased in infected *tert* crispant embryos compared to uninfected *tert* crispants indicating a small global increase in DNA damage in the infection-susceptible *tert* crispants (Figure 4B). However, functional examination of the DNA damage response in *tp53* mutants and *sting* crispants failed to rescue the *tert* knockdown-induced susceptibility to *M. marinum* infection in our embryo infection model suggesting a non-canonical role for Tert in our system(Figure 4C and 4D, Supplementary Figure 3).

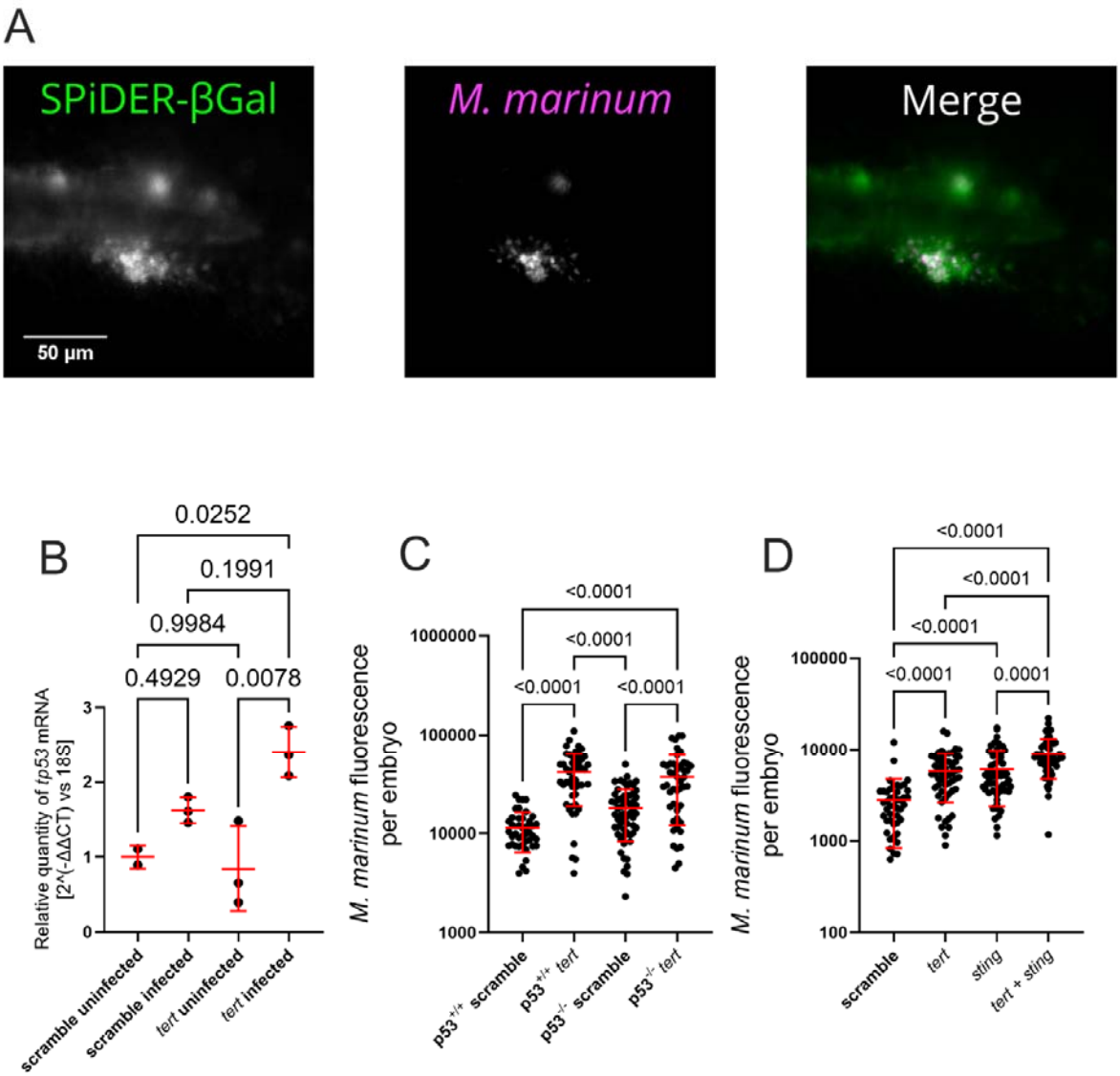

Figure 4: Increased susceptibility to infection in *tert* crispants is not driven by DNA damage response pathways.
(A) Fluorescent SPiDER-βGal staining (green) around *M. marinum* granuloma (magenta) in a 5 dpi embryo.
(B) Quantification of *tp53* transcript abundance in 5 dpi *tert* crispant embryos infected with *M. marinum*.
(C) Quantification of *M. marinum* burden in 5 dpi *tp53* mutant embryos.
(D) Quantification of *M. marinum* burden in 5 dpi *sting* crispant embryos.

Tert supports infection-induced myelopoiesis

Zebrafish *tert* and *terc* are known to be necessary for developmental myelopoiesis (*16, 17, 32, 33*), and *M. marinum* infection control requires replenishment of the myeloid cell compartment (*34*). Conversely, infection with smooth morphotype *M. abscessus* or *M. smegmatis*, two infections that were not exacerbated by Tert depletion, did not induce myelopoiesis in zebrafish embryos (Supplementary Figure 4A and 4B). Furthermore, we did not observe a specific leukocytic response to the sites of CHIKV replication correlating

Tert-dependent immunity with severe infections that drive infection-induced myelopoiesis (Supplementary Figure 4C).

We next analyzed infection-induced myelopoiesis as a potential mechanism of susceptibility in *tert* crispants using *Tg(lyzc:GFP)*^{nz117} and *Tg(lyzc:dsred)*^{nz50} lines, where neutrophils are fluorescently labelled (*35*), and the *TgBAC(mpeg1.1:EGFP)*^{vcc7} line where macrophages are fluorescently labelled (*36*). Caudal hematopoietic tissue-resident neutrophil and macrophages were reduced in *tert* crispants late in infection (Figure 5A and 5B).

To establish if the loss of *lyzc* and *mpeg1.1* positive cells was due to reduced haematopoietic stem cell (HSC) numbers or a lack of differentiation of myeloid cells, we enumerated *Tg(Mmu.Runx1:NLS-mCherry)*^{cz2010} positive HSCs (Figure 5C) (*37*). Tert crispants exhibited a decline in HSC counts at 5 dpi, corresponding with the observed loss of myeloid cells.

Genetic supplementation of endogenous *tert* by microinjection with mRNA encoding full length and catalytically dead zebrafish *tert* increased neutrophil numbers late in infection (Figure 5D). This increase in leukocyte number corresponded with protection from infection (Figure 3C) placing Tert in the control pathogenic mycobacterial infection via supporting infection-induced myelopoiesis.

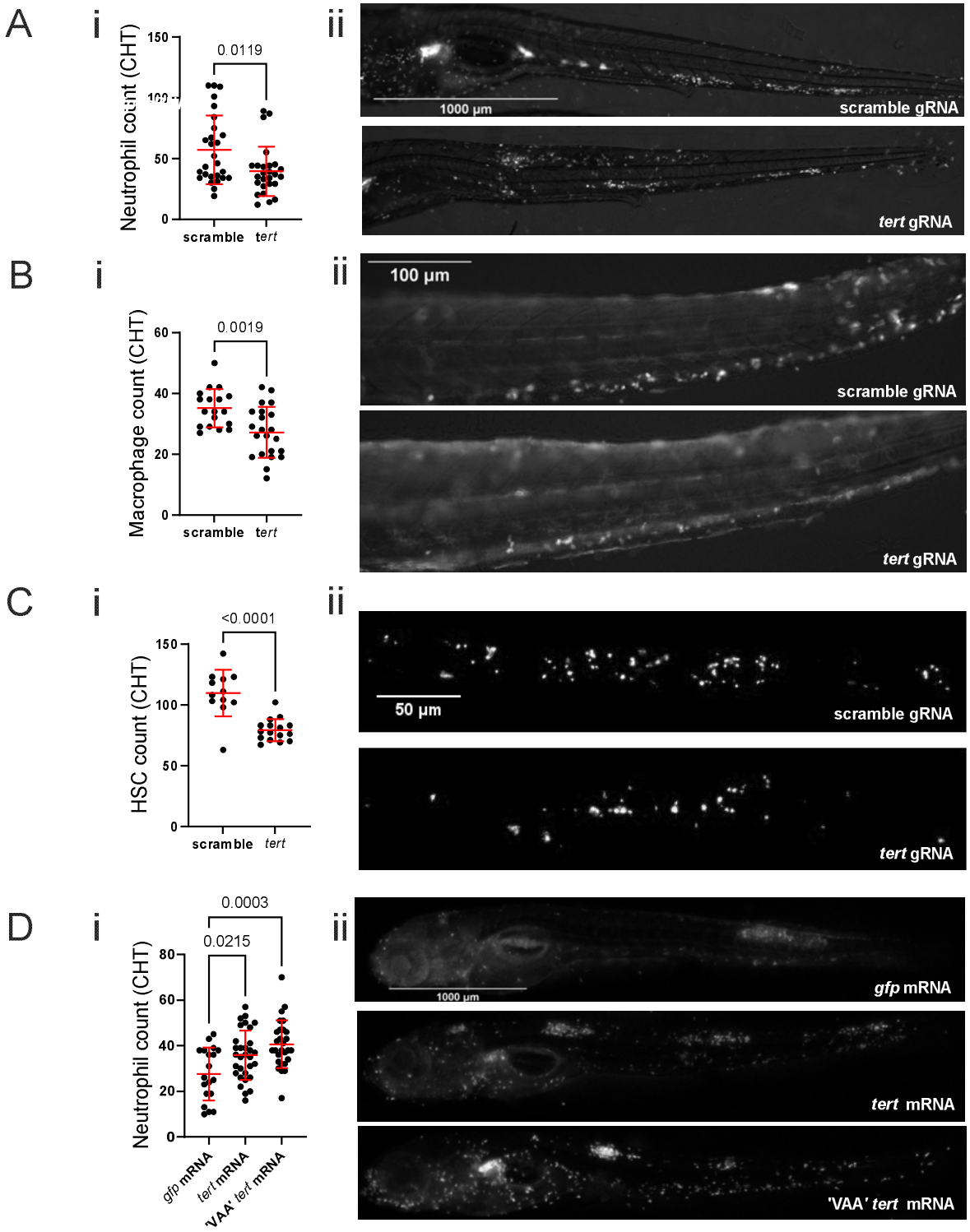

Figure 5: Expression of *tert* correlates with infection demand-driven leukocyte abundance. (A) i. Quantification of CHT-resident neutrophils in 5 dpi *Tg(lyzC:dsred) tert* crispant embryos infected with *M. marinum*. ii. Representative images of fluorescent neutrophils. Bracket demarcates CHT region used for counting.

(B) i. Quantification of CHT-resident macrophages in 5 dpi *TgBAC(mpeg1.1:gfp) tert* crispant embryos infected with *M. marinum*. ii. Representative images of fluorescent macrophages in the CHT region.
(C) i. Quantification of CHT-resident HSCs in 5 dpi *Tg(Mmu.Runx1:NLS-mCherry)* embryos infected with *M. marinum*. ii. Representative images of fluorescent HSCs in the CHT region.
(D) i. Quantification of CHT-resident neutrophils in 5 dpi *Tg(lyzC:dsred)* embryos injected with control eGFP, *tert*, or VAA *tert* mRNA and infected with *M. marinum*. ii. Representative images of fluorescent neutrophils.

Discussion

Our study used depletion of zebrafish telomerase reverse transcriptase to find a novel role for telomerase in the control of mycobacterial infection via supporting infection demand-driven myelopoiesis. These data provide a mechanism that may contribute to the increasing susceptibility to TB during ageing and provide a complementary explanation for the association of short LTL with infection susceptibility. The data further suggest supplementation of telomerase or myelopoietic factors could be used to bolster anti-TB immunity in the elderly (*34*).

While disruption of telomerase activity is associated with canonical telomere-shortening, our use of the VAA active site mutant *tert* and CTD *tert* mRNA to curtail *M. marinum* infection points towards a non-canonical function of Tert in infection demand-driven hematopoiesis. We note that although BIBR1532 binds to *Tribolium castaneum* TERT near the nucleotide binding domain, although it is unclear if this causes loss of non-canonical functions in addition the well-documented loss of canonical function (*38*). Furthermore, the mechanism of action for MST-312 remains unknown. We have previously reported a non-canonical role of zebrafish Tert in supporting gut macrophage proliferation in adult animals (*19*), an organ with constant turnover and immune stimulation, and consistent with the defect in infection demand-driven hematopoiesis found in this study. Non-canonical telomerase, non-coding RNA component (TERC), and shelterin functions span a wide range of cellular activities, while there are similarities in the DNA-based themes of these functions there is also clear mechanistic independence of their non-canonical activities (*39, 40*).

Disseminated *M. tuberculosis* drives epigenetic reprogramming of HSCs to impair the myelopoietic response of infection (*41*). Our zebrafish-*M. marinum* infection model data adds to this concept by demonstrating loss of HSCs sensitized by the loss of host telomerase, suggesting TB infection may accelerate the onset of clonal hematopoiesis in the elderly. Our finding that the premature aging model of telomerase deficiency is a susceptibility factor for pathogenic mycobacterial infection ties together with prior human TB and guinea pig-*M. tuberculosis* infection model data finding *M. tuberculosis* infection prematurely ages the host (*4*). Together, these data suggest a vicous cycle whereby TB ages the host triggering a premature decline of hematopoietic function and further reducing the ability of the host to resist infection.
The loss of HSCs in our chronic mycobacterial infection model suggests TERT may safeguard HSCs from infection-induced damage in addition to performing previously described roles as an inflammatory transcription factor (*42*). Although we did not observe bulk effects of *tert* loss on telomere length in our embryos, we must include the possibility that actively dividing HSCs are more susceptible to loss of canonical telomerase activity causing them to enter premature replicative senescence in chronic infection. We have recently identified an immune cell-autonomous role of Tert in supporting STING-TBK1 signaling (*20*), that while conventionally considered to reduce pathogenic Type I Interferon

in chronic murine *M. tuberculosis* infection, may reduce early immune activation in non-murine mycobacterial infection systems (*43*).Further phenotyping of the HSC and macrophage compartment of TERT mutant animals in the context of infection is required to determine the range of roles played by telomerase in protecting HSCs and macrophage-mediated immune defense.

Multiple studies have linked short telomere length as a proxy for reduced telomerase expression to viral infection susceptibility in species as diverse as humans and rock oysters (*5, 10-12, 44*), however little is known about the mechanistic basis for this association. The only prior mechanistic data connecting telomerase to infection susceptibility is the cell-intrinsic hijacking of host telomerase to support viral replication during lytic human cytomegalovirus infection (*45*). Our bacterial infection experiments add a new dimension to the literature documenting interactions between telomerase and infection across host and pathogen species. We hypothesize the relative contributions of HSC and T-MAC telomerase expression will manifest in a disease-specific manner and encourage more investigation of telomerase function in diverse disease settings.

Methods

Animal husbandry

Zebrafish experiments were approved under the A*STAR IACUC protocols 211667 and 221694; Shanghai Public Health and Clinical Center, Fudan University GB/T 35823-2018 and 2022-A002-01; UK Home Office Project License PPL PP5900632. Breeding adults were housed under 14 hour light / 10 hour dark cycles in a 28°C recirculating aquarium. Eggs were produced by natural spawning and embryos were raised in E3 media at 28°C and supplemented with PTU from 24 hours post fertilization.

Bacterial culture

M. abscessus, M. marinum, and *M. smegmatis* were cultured in 7H9 or on 7H10 supplemented with OADC and hygromycin to select for pTEC fluorescent protein plasmids (L. Ramakrishnan, plasmids are available through Addgene https://www.addgene.org/Lalita_Ramakrishnan/). Single cell suspensions of mycobacteria were prepared and frozen at -70°C in aliquots for individual experiments as previously described (*46*).

Viral culture

Chikungunya virus (CHIKV) virus was produced from an infectious clone plasmid containing a duplicated subgenomic promoter driving ZsGreen (*Anthozoa* reef coral fluorescent protein) expression between the non-structural and structural genes. The viral genome was flanked by a CMV and a HDV ribozyme to launch transcription. BHK cells (RRID: CVCL_1914) were transfected with 500 ng of plasmid per well in a 6 well plate using lipofectamine 2000 (Thermofisher). At 3 days post transfection when CPE reaches approximately 40%, supernatant was cleared of cell debris and used to expand CHIKV culture on VeroE6 cells (RRID: CVCL_0574) for 44 hours. Cleared supernatant was tittered by standard plaque assay on VeroE6 cells. VeroE6 and BHK were grown in DMEM high glutamine (Gibco) with 10% FBS (Hyclone).

Infection with fluorescent pathogens and quantification of infection phenotypes by imaging

Zebrafish embryos were infected by microinjection with approximately 200 CFU *M. marinum*, 1000 CFU DESX1 *M. marinum* or *M. abscessus*, or 50 PFU CHIKV. Primary infection was performed by injection into the caudal vein or neural tube above the yolk sac extension at 2 dpf. Infection was assayed by stereomicroscopy of entire immobilized zebrafish embryos on a Nikon SMZ25 stereoscope or an inverted Nikon Eclipse Ti2 at 5

dpi unless otherwise mentioned. Image analysis was performed in ImageJ/FIJI with bacterial fluorescent pixel count (FPC) carried out as previously described (*47*).

HSC counts were carried out on a Zeiss Celldiscoverer 7 (CD7) widefield microscope equipped with a 20x/0.95 plan-apochromat objective and 0.5x tube lens to acquire a 3 Z-stacks every 5 µm.

Protein extraction and quantification

8-15 zebrafish embryos were pooled and manually homogenised with pestle (Sigma BAF650000002-100EA) for protein extraction with 30µL of Pierce IP Lysis Buffer (Thermo Fisher 87787) with 1x Halt Protease and Phosphatase Inhibitor Cocktail (Thermo Fisher 78440) on ice for 30 minutes. Extract was centrifuged at 16,000g for 30 minutes at 4°C. Supernatant were collected and diluted 20 folds before protein concentration was quantified using Pierce™ BCA Protein Assay Kits (Thermo Fisher 23225) in a Tecan plate reader at 562nm. Samples were extracted as pooled triplicates.

Quantitative telomeric repeat amplification protocolThe standard curve was constructed using 1000ng, 200ng, 40ng, 8ng, 1.6ng of protein per experiment and $10^{[(Ct\ sample-Yint)/slope]}$ was used to determine the relative telomerase activity of samples. Per 25µL reaction, 8.5µL of nuclease free water, 12.5µL of 2x PowerUp SYBR Green Master Mix (Thermo Fisher A25742), 1µL of 500ng/µL of TS and ACX primer and 2µL of 500ng of protein extract was used. CFX96 Touch Real-Time PCR Detection System was used to run the following protocol: 30°C for 30 minutes, 95°C for 10 minutes, 40 cycles of 95°C for 15 seconds and 60°C for 1 minute.

In situ hybridization

DIG-labeled RNA antisense probes were synthesized by *in vitro* transcription with DIG-labeled mix (Roche 11277073910) and the MEGA shortscript T7 Transcription kit (Thermo Fisher AM1354) from *tert* cDNA cloned into a pBluescript SK vector (primers referred to as ISH-tert in Table 1). Probe preparation and *in situ* hybridization of paraffin sections were carried out as described (*22*).

CRISPR-Cas9 mutagenesis

Gene-specific oligos for *in vitro* transcription of gRNAs were designed with IDT or selected from Wu *et al*. (*48*). HiScribe T7 High Yield RNA Synthesis Kit (NEB E2040) was used for *in vitro* transcription and Alt-R CRISPR-Cas9 crRNA was purchased commercially (IDT). Alt-R S.p. Cas9 Nuclease V3 (IDT 1081059) was combined with gRNA/crRNA and injected into the yolk of 1-2 cell stage zebrafish embryos.

Small molecule treatment

BIBR1532 (Selleckchem S1186)and MST-312 (Sigma M3949) were dissolved in DMSO. Small molecules were added to the media of infected embryos at final concentrations of 600 nM BIBR1532 and 2.5 µM MST-312. Small molecules were refreshed in complete media changes every second day.

In vitro mRNA synthesis and embryo injection

A full length *tert* cDNA (referred to as FL-tert in Table 1) was cloned into pGEMTeasy using Q5 polymerase (New England Biolabs). This was subcloned into a pSP64 Poly(A) plasmid (Promega P1241) using NEBuilder HiFi DNA Assembly (NEB E2621). Site-directed mutagenesis was carried out with the Q5 Site-Directed Mutagenesis Kit (NEB E0554) to mutate the ATGAT bases to CCGCC resulting in a predicted change in aspartate to alanine recreating the VAA catalytically dead TERT mutation (*49*). *In vitro* transcription of capped

mRNA was performed with mMESSAGE mMACHINE Sp6 Transcription Kit (Invitrogen AM1340).

tert CTD primers (Refer to Table 1) was used to generate a truncated C terminal domain (CTD) *tert* construct from full length *tert* cDNA with Q5 polymerase and KLD enzyme master mix (NEB M0554). *In vitro* transcription of capped mRNA was performed with mMESSAGE mMACHINE Sp6 Transcription Kit (Invitrogen AM1340).

300 pg of mRNA, in 1.5 nL volume, was injected into the yolk of 1-4 cell stage zebrafish embryos.

<u>DNA extraction and telomere length analysis</u>
7-10 embryos were pooled for gDNA extraction using Monarch Spin gDNA Extraction Kit (NEB T3010L) as per manufacturer's protocol with minor adjustments, 2 µL of proteinase K and RNase A was used instead. Samples were extracted as pooled triplicates. Monarch Spin PCR & DNA Cleanup Kit (5 µg) (NEB T1130L) was used to purify and concentrate gDNA.
30 ng of gDNA was used per 10 µL reaction with *rps11* as the single copy gene housekeeper. Per 10 µL reaction, 3.2 µL of nuclease free water, 5 µL of 2x PowerUp SYBR Green Master Mix (Thermo Fisher A25742), 0.4 µL of 10 µM forward and reverse primers and 1 µL of gDNA was used. $2{-}\Delta\Delta Ct$ was used to analysis relative telomere length.

<u>DNA damage assays</u>
SPiDER-βGal staining was carried out with the Cellular Senescence Detection Kit - SPiDER-βGal (Dojindo SG03-10) as per manufacturer's instructions on fixed zebrafish embryos equilibrated to McIlvain buffer pH6 and stained for 30 minutes at 37°C.

<u>RNA extraction</u>
7-25 embryos were pooled for RNA extraction using TRIzol (Thermo Fisher 15596018) or NucleoSpin RNA kit (Macherey-Nagel 740955.250) as per manufacturer's protocol. Samples were extracted as pooled triplicates.

<u>Gene expression analysis</u>
Quantitative PCR was performed with reverse transcription using the High Capacity cDNA Kit (Applied Biosystems 4368813) or SensiFAST cDNA Synthesis Kit (BIO-65054) and PCR amplification with PowerUp SYBR Green Master Mix (Thermo Fisher A25742).

<u>Statistics</u>
Analyses of quantitative data were carried out with Graphpad Prism using T-tests for pairwise comparisons or ANOVA for multiple comparisons. All data are representative of at least 3 biological replicates unless otherwise stated in the captions. Error bars on graphs represent standard deviation.

Acknowledgements
This study was funded by the Singapore Ministry of Health's National Medical Research Council under its individual research grant scheme (OFIRG22jul-0081) to S.H.O., European Research Council Consolidator Grant (772853 - ENTRAPMENT) and Wellcome Discovery Award (226644/Z/22/Z) to S.M., the National Natural Science Foundation of China (82372263 to B.Y; 82402628 to G.L).
The authors thank A*STAR IMCB Zebrafish Core Facility discussions and the LSHTM Biological Services Facility for expert animal husbandry; Dr Sudipto Roy for providing the

tp53 mutant zebrafish line; Drs Miguel Ferreira, Oliver Dreesen, Dennis Kappei, and Maya Jeitany for helpful telomerase discussions; Mostowy lab members for helpful discussions; Ms Terumi Nakashima, and Drs Caroline Wee, Shifeng Xue, and Zhipeng Tai for technical assistance.

Conflict of Interest Statement

The authors have no conflicts of interest to declare.

Data Availability Statement

The data that support the findings of this study are available from the corresponding author upon reasonable request.

Author's Contributions

Darryl JY Han: experimentation, designed experiments, wrote draft
David M Costa: experimentation, designed experiments, approved draft
Geyang Luo: experimentation, approved draft
Kathryn Wright: experimentation, approved draft
Manitosh Pandey: experimentation, approved draft
Denise Wee: experimentation, approved draft
Yao Chen: experimentation, approved draft
Semih Can Akincilar: provided tools, designed experiments, approved draft
Vinay Tergaonkar: provided tools, approved draft
Rajkumar Dorajoo: experimentation, approved draft
Guillaume Carissimo: provided tools, approved draft
Amit Singhal: experimentation, approved draft
Philip M Elks: experimentation, approved draft
Pamela S Ellis: provided tools, approved draft
Catarina M Henriques: provided tools, designed experiments, approved draft
Bo Yan: experimentation, approved draft
Serge Mostowy: experimentation, approved draft
Stefan H Oehlers: conceived study, experimentation, wrote draft

References

1. A. M. Olmo-Fontanez, J. Turner, Tuberculosis in an Aging World. *Pathogens* **11**, (2022).
2. I. M. Orme, Aging and immunity to tuberculosis: increased susceptibility of old mice reflects a decreased capacity to generate mediator T lymphocytes. *J Immunol* **138**, 4414-4418 (1987).
3. J. B. Torrelles *et al.*, The Impact of Aging on the Lung Alveolar Environment, Predetermining Susceptibility to Respiratory Infections. *Front Aging* **3**, 818700 (2022).
4. C. A. Bobak *et al.*, Increased DNA methylation, cellular senescence and premature epigenetic aging in guinea pigs and humans with tuberculosis. *Aging (Albany NY)* **14**, 2174-2193 (2022).
5. S. Cohen *et al.*, Association between telomere length and experimentally induced upper respiratory viral infection in healthy adults. *JAMA* **309**, 699-705 (2013).
6. J. Helby, B. G. Nordestgaard, T. Benfield, S. E. Bojesen, Shorter leukocyte telomere length is associated with higher risk of infections: a prospective study of 75,309 individuals from the general population. *Haematologica* **102**, 1457-1465 (2017).
7. G. A. Dos Santos *et al.*, Shorter leukocyte telomere length is associated with severity of COVID-19 infection. *Biochem Biophys Rep* **27**, 101056 (2021).

8. S. Liu *et al.*, Peripheral blood leukocyte telomere length is associated with survival of sepsis patients. *Eur Respir J* **55**, (2020).
9. L. Freimane *et al.*, Telomere length and mitochondrial DNA copy number in multidrug-resistant tuberculosis. *Tuberculosis (Edinb)* **131**, 102144 (2021).
10. G. A. Noppert *et al.*, Pathogen burden and leukocyte telomere length in the United States. *Immun Ageing* **17**, 36 (2020).
11. A. E. Aiello *et al.*, The impact of pathogen burden on leukocyte telomere length in the Multi-Ethnic Study of Atherosclerosis. *Epidemiol Infect* **145**, 3076-3084 (2017).
12. J. B. Dowd *et al.*, Persistent Herpesvirus Infections and Telomere Attrition Over 3 Years in the Whitehall II Cohort. *J Infect Dis* **216**, 565-572 (2017).
13. P. Katoto *et al.*, Telomere length and outcome of treatment for pulmonary tuberculosis in a gold mining community. *Scientific reports* **11**, 4031 (2021).
14. W. Udomsinprasert *et al.*, Leukocyte telomere length as a diagnostic biomarker for anti-tuberculosis drug-induced liver injury. *Scientific reports* **10**, 5628 (2020).
15. X. Chen *et al.*, Relationship between common telomere length-related genetic variations, telomere length, and risk of antituberculosis drug-induced hepatotoxicity in Chinese Han population: As assessed for causality using the updated Roussel Uclaf Causality Assessment Method. *Fundam Clin Pharmacol* **37**, 858-867 (2023).
16. S. Imamura *et al.*, A non-canonical function of zebrafish telomerase reverse transcriptase is required for developmental hematopoiesis. *PLoS ONE* **3**, e3364 (2008).
17. E. Martinez-Balsalobre *et al.*, Telomerase RNA-based aptamers restore defective myelopoiesis in congenital neutropenic syndromes. *Nat Commun* **14**, 5912 (2023).
18. M. Anchelin, L. Murcia, F. Alcaraz-Perez, E. M. Garcia-Navarro, M. L. Cayuela, Behaviour of telomere and telomerase during aging and regeneration in zebrafish. *PLoS ONE* **6**, e16955 (2011).
19. P. S. Ellis *et al.*, A subset of gut leukocytes has telomerase-dependent "hyper-long" telomeres and require telomerase for function in zebrafish. *Immun Ageing* **19**, 31 (2022).
20. S. C. Akincilar *et al.*, Evolutionarily conserved role of telomerase reverse transcriptase in programming the microenvironment via regulation of the cGAS–STING pathway. *Nature Cell Biology*, (2025).
21. M. R. Cronan *et al.*, A non-canonical type 2 immune response coordinates tuberculous granuloma formation and epithelialization. *Cell* **184**, 1757-1774 e1714 (2021).
22. G. Luo *et al.*, Temporal and cellular analysis of granuloma development in mycobacterial infected adult zebrafish. *J Leukoc Biol* **115**, 525-535 (2024).
23. N. Palha *et al.*, Real-time whole-body visualization of Chikungunya Virus infection and host interferon response in zebrafish. *PLoS Pathog* **9**, e1003619 (2013).
24. A. Amin *et al.*, Short-Term TERT Inhibition Impairs Cellular Proliferation via a Telomere Length-Independent Mechanism and Can Be Exploited as a Potential Anticancer Approach. *Cancers* **15**, (2023).
25. S. Giunco *et al.*, Anti-Proliferative and Pro-Apoptotic Effects of Short-Term Inhibition of Telomerase In Vivo and in Human Malignant B Cells Xenografted in Zebrafish. *Cancers* **12**, (2020).
26. P. Ilmonen, A. Kotrschal, D. J. Penn, Telomere attrition due to infection. *PLoS ONE* **3**, e2143 (2008).
27. S. Liu *et al.*, Mycobacterium tuberculosis suppresses host DNA repair to boost its intracellular survival. *Cell Host Microbe* **31**, 1820-1836 e1810 (2023).
28. M. Anchelin *et al.*, Premature aging in telomerase-deficient zebrafish. *Dis Model Mech* **6**, 1101-1112 (2013).

29. C. M. Henriques, M. C. Carneiro, I. M. Tenente, A. Jacinto, M. G. Ferreira, Telomerase is required for zebrafish lifespan. *PLoS Genet* **9**, e1003214 (2013).
30. N. Serifoglu *et al.*, cGAS-STING are responsible for premature aging of telomerase-deficient zebrafish. *EMBO J*, (2025).
31. N. Serifoglu, B. Lopes-Bastos, M. G. Ferreira, Lack of telomerase reduces cancer incidence and increases lifespan of zebrafish tp53(M214K) mutants. *Scientific reports* **14**, 5382 (2024).
32. F. Alcaraz-Perez *et al.*, A non-canonical function of telomerase RNA in the regulation of developmental myelopoiesis in zebrafish. *Nat Commun* **5**, 3228 (2014).
33. J. Garcia-Castillo *et al.*, Telomerase RNA recruits RNA polymerase II to target gene promoters to enhance myelopoiesis. *Proc Natl Acad Sci U S A* **118**, (2021).
34. A. J. Pagan *et al.*, Myeloid Growth Factors Promote Resistance to Mycobacterial Infection by Curtailing Granuloma Necrosis through Macrophage Replenishment. *Cell Host Microbe* **18**, 15-26 (2015).
35. C. Hall, M. V. Flores, T. Storm, K. Crosier, P. Crosier, The zebrafish lysozyme C promoter drives myeloid-specific expression in transgenic fish. *BMC Dev Biol* **7**, 42 (2007).
36. K. Sugimoto, S. P. Hui, D. Z. Sheng, M. Nakayama, K. Kikuchi, Zebrafish FOXP3 is required for the maintenance of immune tolerance. *Dev Comp Immunol* **73**, 156-162 (2017).
37. O. J. Tamplin *et al.*, Hematopoietic stem cell arrival triggers dynamic remodeling of the perivascular niche. *Cell* **160**, 241-252 (2015).
38. C. Bryan *et al.*, Structural Basis of Telomerase Inhibition by the Highly Specific BIBR1532. *Structure* **23**, 1934-1942 (2015).
39. S. C. Akincilar, C. H. T. Chan, Q. F. Ng, K. Fidan, V. Tergaonkar, Non-canonical roles of canonical telomere binding proteins in cancers. *Cell Mol Life Sci* **78**, 4235-4257 (2021).
40. C. Cao *et al.*, Canonical and non-canonical functions of the non-coding RNA component (TERC) of telomerase complex. *Cell Biosci* **15**, 30 (2025).
41. N. Khan *et al.*, M. tuberculosis Reprograms Hematopoietic Stem Cells to Limit Myelopoiesis and Impair Trained Immunity. *Cell* **183**, 752-770 e722 (2020).
42. A. Ghosh *et al.*, Telomerase directly regulates NF-kappaB-dependent transcription. *Nat Cell Biol* **14**, 1270-1281 (2012).
43. C. W. Munson, D. Kaushal, Type I interferons in tuberculosis pathogenesis and prevention. *Trends Microbiol*, (2025).
44. A. Dupoue *et al.*, Reproductive aging weakens offspring survival and constrains the telomerase response to herpesvirus in Pacific oysters. *Sci Adv* **10**, eadq2311 (2024).
45. C. M. Cavanaugh *et al.*, Effect of host telomerase inhibition on human cytomegalovirus. *J Virol* **99**, e0157824 (2025).
46. K. Takaki, J. M. Davis, K. Winglee, L. Ramakrishnan, Evaluation of the pathogenesis and treatment of Mycobacterium marinum infection in zebrafish. *Nat Protoc* **8**, 1114-1124 (2013).
47. M. A. Matty, S. H. Oehlers, D. M. Tobin, Live Imaging of Host-Pathogen Interactions in Zebrafish Larvae. *Methods Mol Biol* **1451**, 207-223 (2016).
48. R. S. Wu *et al.*, A Rapid Method for Directed Gene Knockout for Screening in G0 Zebrafish. *Dev Cell* **46**, 112-125 e114 (2018).
49. W. C. Drosopoulos, V. R. Prasad, The active site residue Valine 867 in human telomerase reverse transcriptase influences nucleotide incorporation and fidelity. *Nucleic Acids Res* **35**, 1155-1168 (2007).

50. A. T. McCurley, G. V. Callard, Characterization of housekeeping genes in zebrafish: male-female differences and effects of tissue type, developmental stage and chemical treatment. *BMC Mol Biol* **9**, 102 (2008).
51. C. Gerri *et al.*, Hif-1alpha regulates macrophage-endothelial interactions during blood vessel development in zebrafish. *Nat Commun* **8**, 15492 (2017).
52. B. Novoa *et al.*, Rag1 immunodeficiency-induced early aging and senescence in zebrafish are dependent on chronic inflammation and oxidative stress. *Aging Cell* **18**, e13020 (2019).
53. R. M. Cawthon, Telomere measurement by quantitative PCR. *Nucleic Acids Res* **30**, e47 (2002).
54. B. S. Herbert, A. E. Hochreiter, W. E. Wright, J. W. Shay, Nonradioactive detection of telomerase activity using the telomeric repeat amplification protocol. *Nat Protoc* **1**, 1583-1590 (2006).

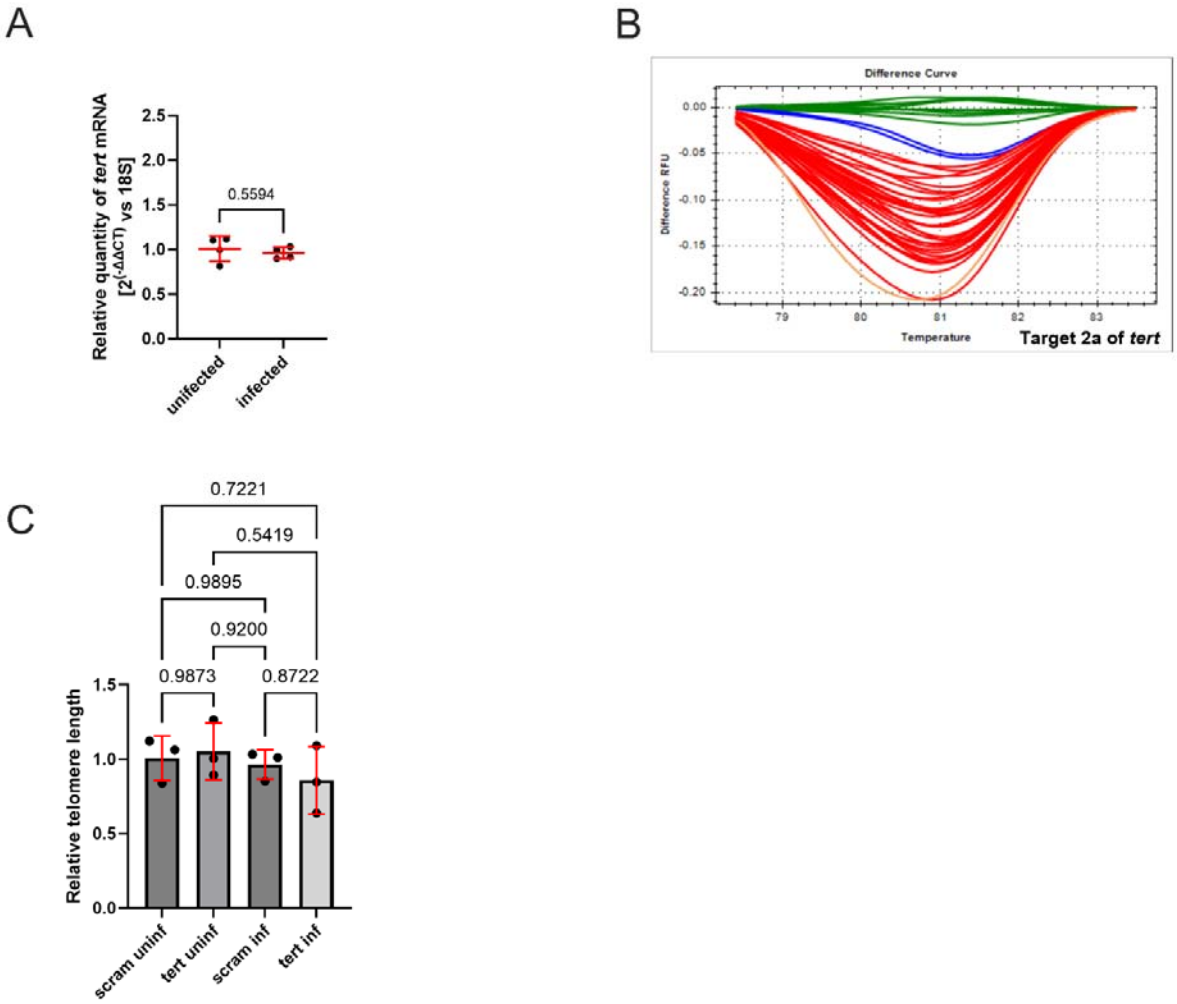

Supplementary Figure 1: Quantification of *tert* and editing efficiency of pooled gRNA-Cas9 editing of *tert*.
(A) Quantification of *tert* in 5 dpi embryos infected with *M. marinum.*
(B) High resolution melt analysis of *tert* gRNA2 target site, n=35, 100% efficiency, control clusters: Green & Blue.
(C) Quantification of telomere length by qPCR from homogenates of 5 dpi embryos infected with *M. marinum*.

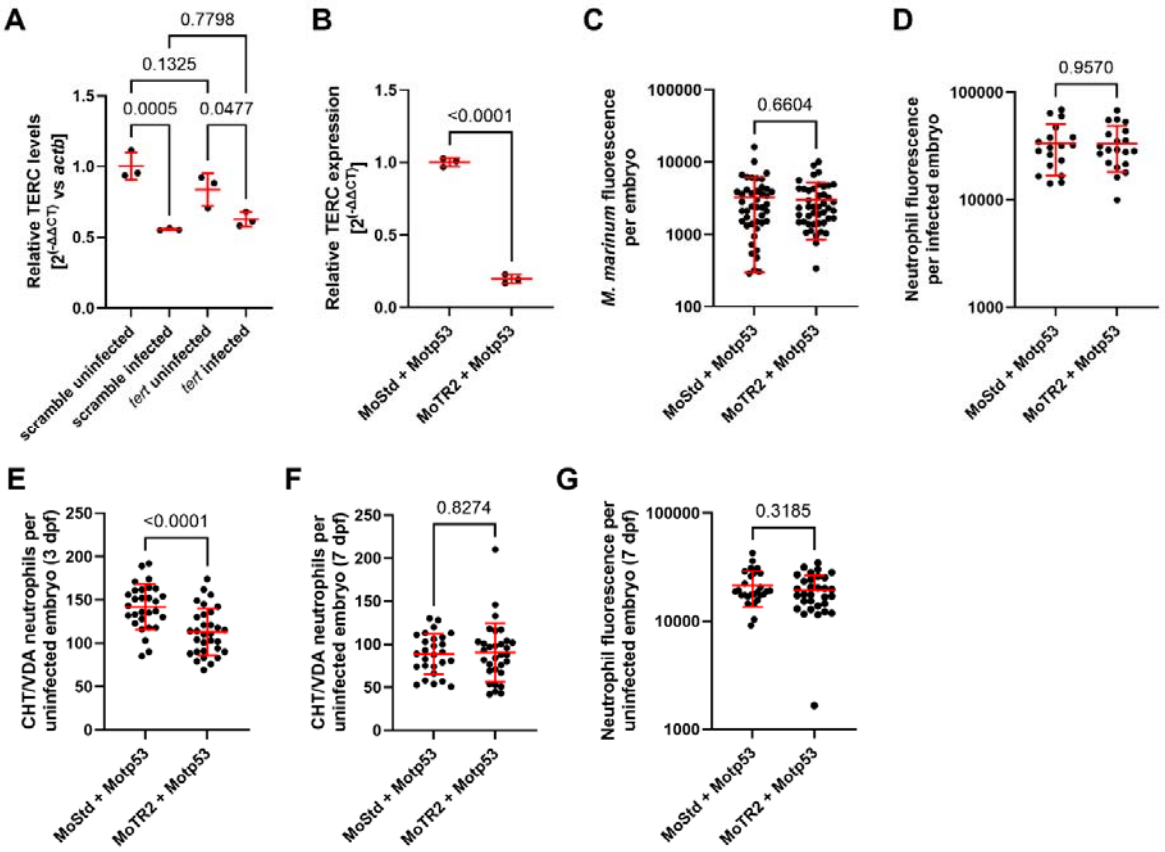

Supplementary Figure 2: Infection-induced reduction in TERC does not correlate with mycobacterial infection susceptibility in zebrafish embryos

(A) Quantification of TERC by qRT-PCR in 5 dpi *tert* crispant embryos infected with *M. marinum*.

(B) Quantification of TERC by qRT-PCR in 5 dpi morpholino-injected embryos infected with *M. marinum*.

(C) Quantification of *M. marinum* burden in 5 dpi morpholino-injected embryos infected with *M. marinum*.

(D) Quantification of total neutrophils in 5 dpi morpholino-injected embryos infected with *M. marinum*.

(E) Quantification of CHT region neutrophils in 3 days post fertilization morpholino-injected embryos.

(F) Quantification of CHT region neutrophils in 7 days post fertilization morpholino-injected embryos.

(G) Quantification of total neutrophils in 7 days post fertilization morpholino-injected embryos.

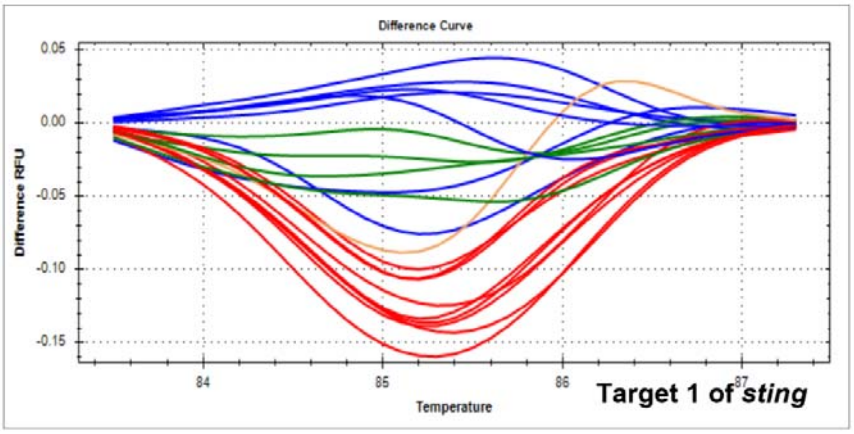

Supplementary Figure 3: Editing efficiency of pooled gRNA-Cas9 editing of *sting*. High resolution melt analysis of *sting* gRNA1 target site, n=18, 77.77% efficiency, control clusters: Green & Blue.

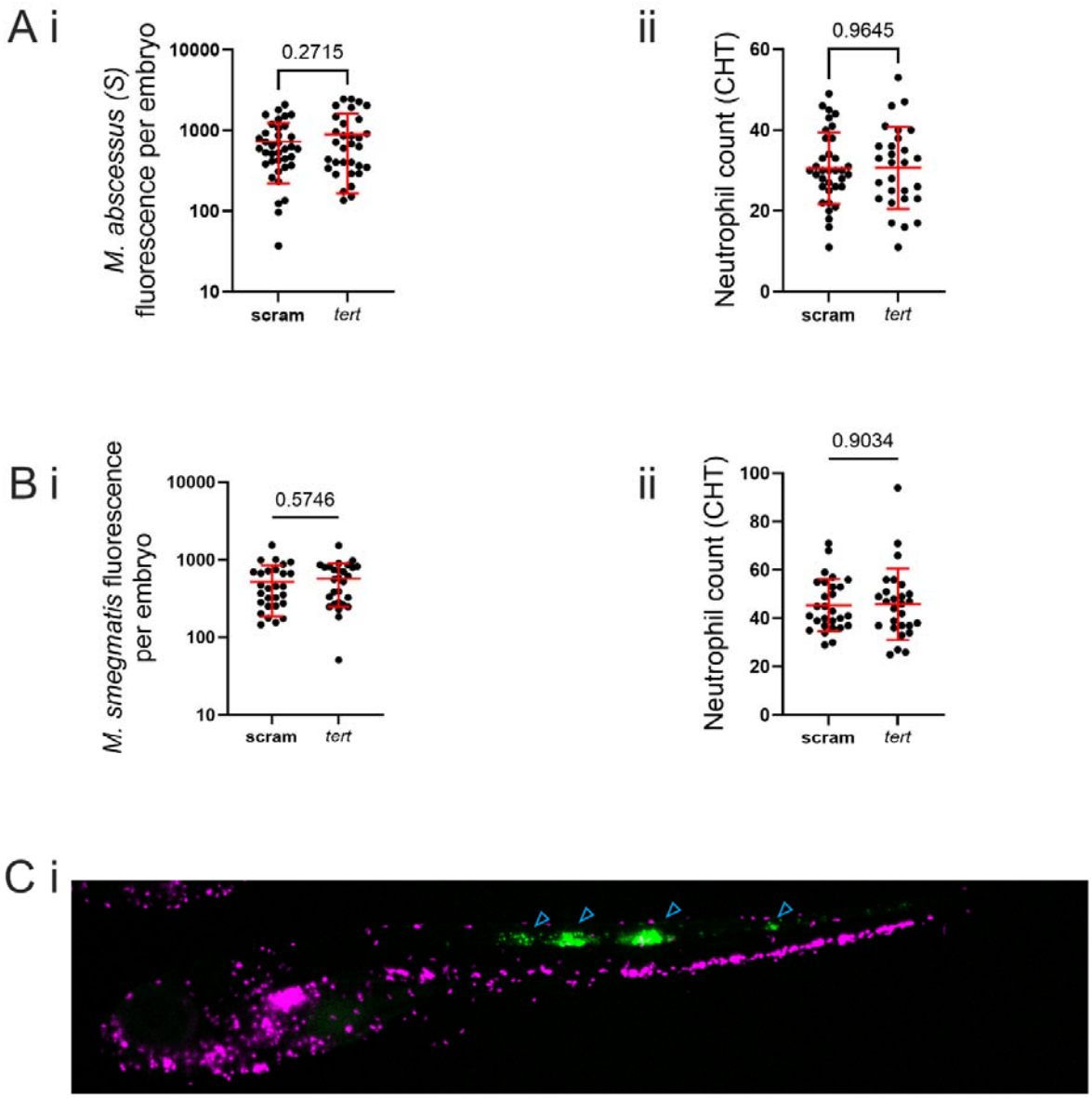

Supplementary Figure 4: Tert-insensitive infection models do not induce demand-driven myelopoiesis

(A) i. Quantification of smooth *M. abscessus* burden in 6 dpi *tert* crispant embryos. ii. Quantification of CHT-resident neutrophils in 6 dpi *Tg(lyzC:dsred) tert* crispant embryos infected with smooth *M. abscessus*.

(B) i. Quantification of *M. smegmatis* burden in 6 dpi *tert* crispant embryos. ii. Quantification of CHT-resident neutrophils in 6 dpi *Tg(lyzC:dsred) tert* crispant embryos infected with *M. smegmatis*.

(C) Representative image of neutrophils (magenta) and CHIKV-infected cells (green, indicated by blue arrowheads) in a 3 dpi *Tg(lyzC:dsred)* embryo.

697 Table 1: Oligonucleotides

Use	Name	Sequence 5′-3′	Reference/notes
Cloning eGFP	eGFP Fw	acacatataccttcatacttaattgtcaagTTATTTGTATAGTTCATCCATGCCATGTG	This study, upper case letters indicate coding sequence
Cloning eGFP	eGFP Fw	ctctgcaaagcaagagattaataacccatcATGAGTAAAGGAGAAGAACTTTTCACTG	This study, upper case letters indicate coding sequence
Cloning full length zebrafish *tert* transcript for IVT	FL-Tert Fw	TAAGCATGTCTGGACAGTACTCGACAGATG	This study
Cloning full length zebrafish *tert* transcript for IVT	FL-Tert Rv	CAGGTTTTTTTTACACCCGC	This study
Cloning full length zebrafish *tert* transcript for ISH	ISH-Tert Fw	caagagattaataacccatcATGTCTGGACAGTACTCGACAGAT	This study, upper case letters indicate coding sequence
Cloning full length	ISH-Tert Rv	cttcatacttaattgtcaagTTACACCCGCATGCTGAAATCCAG	This study, upper

zebrafish *tert* transcript for ISH			case letters indicate coding sequence
Gene expression *actb*	Bactin 1 qFW	CGAGCAGGAGATGGGAACC	McCurley and Callard (*50*)
Gene expression *actb*	Bactin 1 qRv	CAACGGAAACGCTCATTGC	McCurley and Callard (*50*)
Gene expression *actb*	Bactin 1 qFw2	GGAGATGATGCCCCTCGTG	This study
Gene expression *actb*	Bactin 1 qRv2	GGAGATGATGCCCCTCGTG	This study
Gene expression *18s*	18s qFw	TCGCTAGTTGGCATCGTTTATG	Gerri *et al.* (*51*)
Gene expression *18s*	18s qRv	CGGAGGTTCGAAGACGATCA	Gerri *et al.* (*51*)
Gene expression *tert*	tert qFw	GCGCTCCTTATATCCAGTCG	This study
Gene expression *tert*	tert qRv	GGCGCATACAATAAGTCCACT	This study
Gene expression *tp53*	tp53 qFw	GATGGTGAAGGACGAAGGAA	Novoa *et al.* (*52*)
Gene expression *tp53*	tp53 qRv	AAATGACCCCTGTGACAAGC	Novoa *et al.* (*52*)
Gene expression cdkn1a	cdkn1a qFw	AACGCTGCTACGAGACGAAT	Novoa *et al.* (*52*)
Gene	cdkn1a	CGCAAACAGACCAACATCAC	Novoa

expression cdkn1a	qRv		*et al.* (*52*)
Gene expression TERC	TERC qFw	TTCCGCGGTTTCGATACTTT	This study
Gene expression TERC	TERC qRv	CCACAGACCTGCCGAATGT	This study
Gene expression *rps11*	rps11 Ex5 Fw	AGGTGACATCGTTACAGTTGGA	This study
Gene expression *rps11*	rps11 Ex5 Rv	GGAACTGCTTCTTGGCTCCA	This study
Gene expression telomere	telom-Fw	GGTTTTTGAGGGTGAGGGTGAGGGTGAGGGTGAGGGT	Cawthon (*53*)
Gene expression telomere	telom-Rv	TCCCGAACTATCCCTATCCCTATCCCTATCCCTATCCCTA	Cawthon (*53*)
gRNA scaffold	sgRNA Scaffold Primer	AAAAGCACCGACTCGGTGCCACTTTTTCAAGTTGATAACGGACTAGCCTTATTTTAACTTGCTATTTCTAGCTCTAAAAC	Wu *et al*. (*48*)
gRNA Scrambled	scramble_target_1	TAATACGACTCACTATAGGCAGGCAAAGAATCCCTGCCGTTTTAGAGCTAGAAATAGC	Wu *et al*. (*48*)
gRNA Scrambled	scramble_target_2	TAATACGACTCACTATAGGTACAGTGGACCTCGGTGTCGTTTTAGAGCTAGAAATAGC	Wu *et al*. (*48*)
gRNA Scrambled	scramble_target_3	TAATACGACTCACTATAGGCTTCATACAATAGACGATGGTTTTAGAGCTAGAAATAGC	Wu *et al*. (*48*)
gRNA Scrambled	scramble_target_4	TAATACGACTCACTATAGGTCGTTTTGCAGTAGGATCGGTTTTAGAGCTAGAAATAGC	Wu *et al*. (*48*)
gRNA *sting*	sting_Target_1	TAATACGACTCACTATAGGGACTGGGTTTTCTTACTCGTTTTAGAGCTAGAAATAGC	Wu *et al*. (*48*)
gRNA *sting*	sting_Target_2	TAATACGACTCACTATAGGCATGTTGCTCAATAGCCTGTTTTAGAGCTAGAAATAGC	Wu *et al*. (*48*)
gRNA *sting*	sting_Target_3	TAATACGACTCACTATAGGCAGAAGGATATGTAGACGGTTTTAGAGCTAGAAATAGC	Wu *et al*. (*48*)

gRNA *sting*	sting_Target_4	TAATACGACTCACTATAGGAGTTTCTCACCGTTGAGCGTTTTAGAGCTAGAAATAGC	Wu *et al*. (*48*)
gRNA *tert*	tert_Target_1	TAATACGACTCACTATAGGAACCGGCTTTCGGCCGTCGTTTTAGAGCTAGAAATAGC	Wu *et al*. (*48*)
gRNA *tert*	tert_Target_2	TAATACGACTCACTATAGGACATTGCGAGGGTCGAGGGTTTTAGAGCTAGAAATAGC	Wu *et al*. (*48*)
gRNA *tert*	tert_Target_3	TAATACGACTCACTATAGGGCAGCCCCAGAGCTCGTGGTTTTAGAGCTAGAAATAGC	Wu *et al*. (*48*)
gRNA *tert*	tert_Target_4	TAATACGACTCACTATAGGTTCAGGCCTGCCATTGGCGTTTTAGAGCTAGAAATAGC	Wu *et al*. (*48*)
HRM *sting*	HRM_Sting_Fw	CTGTGATGGGAGAAGACGCT	This study
HRM *sting*	HRM_Sting_Rv	TCACTGAACTTGTCTGAGTCCA	This study
HRM *tert*	HRM_Tert_Fw	GTTGGAAACCAGCGGATCAG	This study
HRM *tert*	HRM_Tert_Rv	AGGAAGTTCTTCATGCCCCG	This study
ISH probe *tert*	ISH_Tert_Fw	TGGCGGATTCAGGCCGGTTTTG	This study
ISH probe *tert*	ISH_Tert_Rv	TATTGAACATTGCGAGGGTCGAG	This study
Site directed mutagenesis of zebrafish *tert* transcript	SDM Tert 'AA' Fw	GAGGCTGATTG[CCGCC]TTTTTGCTCATTACTCC	This study, bracketed sequence indicates mutant sequence
Site directed mutagenesis of zebrafish *tert* transcript	SDM Tert 'AA' Rv	ATCAGACACCCTCCTTTAG	This study
Site directed mutagenesis	tert CTD Fw	CATGATGGGTTATTAATCTCTTGCTTTG	This study

deletion of zebrafish *tert* transcript			
Site directed mutagenesis deletion of zebrafish *tert* transcript	tert CTD Rv	GGCTCCGCCCACTCTC	This study
qTRAP primer	ACX	GCGCGGCTTACCCTTACCCTTACCCTAACC	Herbert *et al* (*54*)
qTRAP primer	TS	AATCCGTCGAGCAGAGTT	Herbert *et al* (*54*)

698
699